# Spectroscopic Characterization of Distortion in Enzyme Complexes

Paul R. Carey*

*Department of Biochemistry, Case Western Reserve University, 10900 Euclid Avenue, Cleveland, Ohio 44106*

*Received November 23, 2005*

## *Contents*

1. Introduction 3043
   1.1. Distortion 3043
   1.2. Why Vibrational Spectroscopy? 3043
2. Distortion at Carbonyl Groups 3044
   2.1. Overview 3044
   2.2. Serine Proteases 3044
   2.3. Meisenheimer Formation in a Dehalogenase 3045
   2.4. Pyruvate in Lactate Dehydrogenase 3046
   2.5. Michaelis Complex in Liver Alcohol Dehydrogenase 3046
   2.6. Uracil DNA Glycosylase—Distortion? 3047
3. Distortion at Phosphate and Vanadate Groups 3047
   3.1. Bond Length–Bond Strength–Vibrational Frequency Relationships 3047
   3.2. Phosphoglucomutase 3047
   3.3. Purine Nucleoside Phosphorylase 3048
4. Distortion within $\pi$-Electron Systems 3049
   4.1. Acyl Papains 3049
   4.2. Acyl Thiosubtilisn and Selenosubtilisin 3049
   4.3. Contribution of Electronic Strain in Enoyl-CoA Hydratase 3050
5. Distortion Involving Torsional Angles 3051
   5.1. Distortion toward the Transition State in Dithioacyl Papains 3051
   5.2. Distortion in a $\beta$-Lactamase–Tazobactam Reaction Intermediate 3052
6. Acknowledgments 3053
7. References 3053

Paul Carey obtained his B.Sc. (chemistry) and D.Phil. (chemical applications of NMR) at the University of Sussex, England. Prompted by his postdoctoral mentor, Harold Bernstein, at the National Research Council of Canada in Ottawa, he changed fields and started to use Raman spectroscopy to characterize biological systems. He became a research scientist at the NRC in 1971. In 1994 he moved to Case Western Reserve University, where he is now Professor of Biochemistry and Chemistry and Director of the Cleveland Center for Structural Biology. It has been his great fortune that technical advances in the Raman field have enabled the Carey group to tackle areas in biochemistry that were just "a glint in the eye" and totally inaccessible at the beginning of the laser era.

## *1. Introduction*

### 1.1. Distortion

A molecule in its lowest energy (ground) state usually is defined by a unique set of atomic coordinates and by the distribution of electrons in its chemical bonds. When a substrate molecule binds to an enzyme's active site, any perturbation from the ground-state coordinates or electron distribution constitutes distortion. At the same time substrate−active site interactions perturb the properties of the protein in some manner and this can be described as distortion of the protein. This review describes how distortion can be quantitated using vibrational spectroscopy and, in a more challenging undertaking, how it can sometimes be related to catalytic efficacy. Several biophysical techniques have been used to probe for distortion within proteins. For example, by analyzing the X-ray structures of 75 proteins refined at 1.75 Å or better, Karplus[1] cataloged the presence of N−Cα−C bond angles deviating by up to 5° from the standard value, leading to the proposition that these deviant bonds occurred in strained regions of the protein. Magnetic resonance measurements have also been used to define distortion. For example, for bacteriorhodopsin[2] they have been used to distinguish between protein conformational change and torsional strain in the Schiff's base chromophore. However, there have not been extensive studies by these methods on viable enzyme−substrate complexes. By way of contrast, vibrational spectroscopy does lend itself to characterizing distortion at the level needed to probe enzyme mechanisms. The reasons for this are outlined in the next section.

### 1.2. Why Vibrational Spectroscopy?

When discussing relationships between structure and reactivity, it becomes apparent that very small changes in structure, e.g. changes of less than 0.01 Å in a bond length, can be associated with large changes (orders of magnitude) in reactivity. The overarching advantage of vibrational spectroscopy is that it can quantitate very small changes in geometries—of less than 0.01 Å in bond lengths, for example. Such precision is usually beyond the reach of techniques such as macromolecular X-ray crystallography and NMR. Vibrational spectroscopy can also provide unique insight into the forces acting on individual groups in active sites. The best

* Telephone: 216 368 0031. Fax: 216 368 3419. E-mail: paul.carey@case.edu.

10.1021/cr0502854 CCC: $59.00 
Published on Web 07/06/2006

studied example is the C═O functional group; in favorable cases it is possible to relate the observed shift in frequency upon binding to the enzyme to the effective hydrogen bonding strength at the C═O group. Another advantage of vibrational spectroscopy stems from the inherent time scale of the physical processes that give rise to infrared absorption or Raman scattering. The time scale is picoseconds or less. Thus, an infrared or Raman spectrum of a sample is essentially an instantaneous "snapshot" of all the molecules making up that sample; effects such as line broadening due to rapid chemical exchange are not observed. This facilitates spectral interpretation when short-lived enzyme substrate complexes are being characterized.

Raman and FTIR spectroscopies share the property that "peak" positions in the spectra are a property solely of the electronic ground state. This is especially advantageous in the resonance Raman technique, where the electronic ground state can be probed exclusively by peak positions whereas peak intensities provide information on excited electronic states. Thus, it is possible to keep excited-state and ground-state effects separate in any discussion of distortion in an enzyme complex. Recently, it has been shown that normal (nonresonance) Raman difference spectroscopy can be undertaken in single protein crystals, allowing the characterization of ligand binding and even slow chemical reactions in the crystals.[3] These experiments offer great synergy with X-ray crystallographic studies of the same systems; the X-ray data provide "the big picture" of conformation while the spectroscopic approach allows the observer to follow chemical events in the crystal in real time. Together they can offer unparalleled insight into distortion.

## *2. Distortion at Carbonyl Groups*

### 2.1. Overview

Carbonyl groups as part of substrates within enzyme active sites have been early subjects for both FTIR[4] and Raman analysis[5] in order to probe the chemistry associated with that group. This interest stems from the facts that, from the mechanistic standpoint, the C═O is often a very important functional group and that the symmetric stretching vibration, $\nu_{C=O}$, is often (but not always) a good group frequency; that is, the vibration is essentially localized at the C═O atoms. Moreover, the location of $\nu_{C=O}$ in the vibrational spectrum occurs in a window in water's IR absorbance permitting detection by FTIR. The group frequency of the C═O stretch can lead to facile interpretation, at least at a simple descriptive level. However, a more complete analysis of the data can lead to accurate quantitative relationships between the geometry of the C═O, active site forces acting on this group and the degree of rate acceleration for the reaction being analyzed.

When citing spectroscopic data as evidence for distortion, it is important to define a standard state. The C═O stretching frequency is the classic example. A shift in the position of the C═O frequency has been taken as evidence for distortion, namely a change in polarization of the C═O group. A shift to lower frequency means the C═O is acquiring more single bond character and has become more polarized; that is, valence bond form II is becoming increasingly important

$$\underset{\text{I}}{>C{=}O} \leftrightarrow \underset{\text{II}}{>C^{+}{-}O^{-}}$$

Of course, in many reactions, this has catalytic significance since form II is more prone to nucleophilic attack. But the key question is, "The C═O shifts—but compared to what?" A suitable standard state is often the substrate in a non-hydrogen bonding solvent such as carbon tetrachloride, which, as far as polarizing forces are concerned, is close to *in vacuo*. If the substrate in aqueous solution is taken as the standard state, then on average the C═O will be experiencing two medium strength H-bonds from water molecules and any shift seen upon binding to the enzyme reflects the fact that the standard state already has a moderately polarized C═O and the shift is measuring the difference between this and the degree of polarization achieved by active site forces. Obviously, consideration of the standard state is of prime importance when using shifts in C═O frequency to quantitate polarizing forces in active sites and in correlating these with rate acceleration.

### 2.2. Serine Proteases

A paradigm for the kind of relationships that can be developed concerns the deacylation step for intermediates of the type

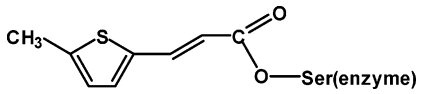


where "enzyme" is either the serine protease subtilisin or chymotrypsin and the acyl group, 5-methylthienyl acryloyl-(5-MTA), is from a non-natural substrate designed to give resonance (intensity-enhanced) Raman spectra with laser excitation near 350 nm. It is possible to purify large amounts (tens of milligrams) of the stable acyl enzyme at pH 3. Using a rapid flow−rapid mixing system, the pH is then jumped to around pH 9, which is the region of the maximum deacylation rate. The resonance Raman spectrum is recorded from the flow mixture before significant deacylation occurs. This provides the C═O stretching frequency as that group is being prepared for nucleophilic attack (for more details, see ref 6 and references therein). As can be seen in Figure 1, throughout the series of acyl enzymes with widely varying reactivity,

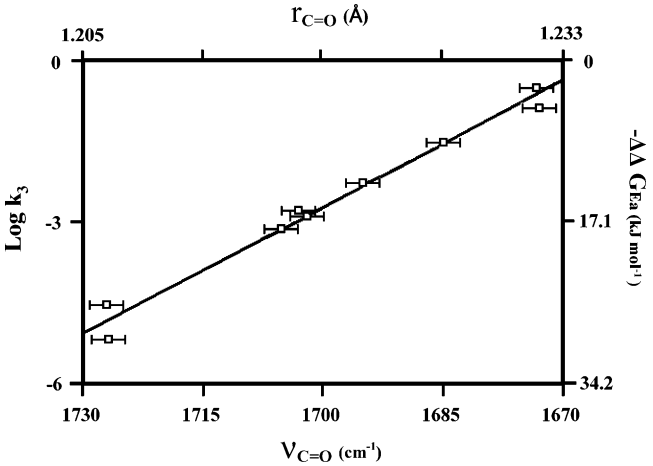


**Figure 1.** Correlation between the carbonyl stretching frequency, $\nu_{C=O}$, and log $k_3$, where $k_3$ is the maximal deacylation rate at pH 10 for the series of acyl serine proteases. Each point represents an acyl enzyme; $\nu_{C=O}$ and $k_3$ are also recast in the forms of $r_{C=O}$ (carbonyl bond length) and $\Delta\Delta G$ (free energy of activation for deacylation), respectively. Reprinted with permission from ref 6. Copyright 1995 American Chemical Society.

**Scheme 1. 4-Chlorobenzoyl CoA Dehalogenase Reaction Pathway**

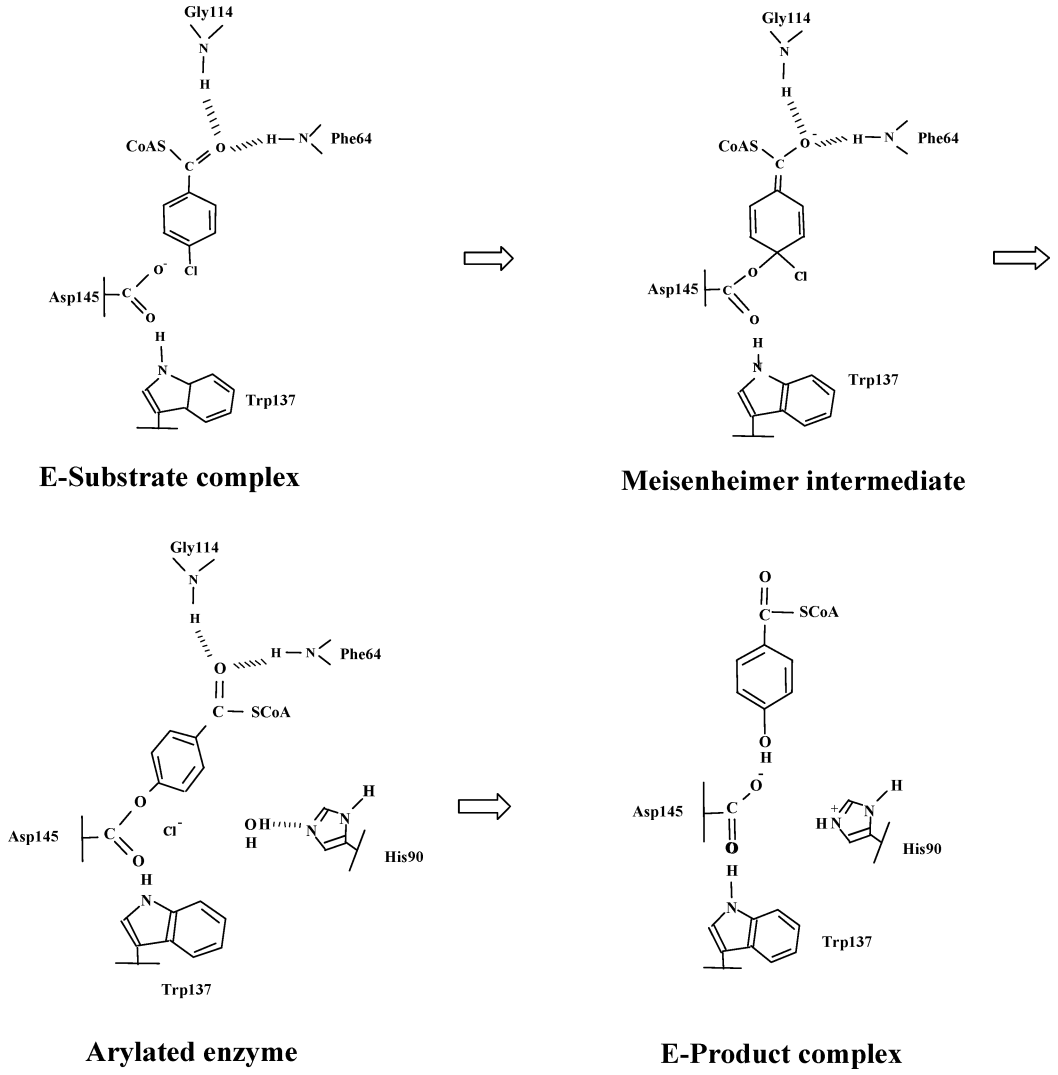


there is a strong correlation between the position of $\nu_{C=O}$ in the resonance Raman spectrum and the log of the deacylation rate constant, $k_3$. Increasing $k_3$ by about 16 300-fold is accompanied by a downshift in $\nu_{C=O}$ of 54 $cm^{-1}$.

Using empirical relationships, these data can be extended in two directions. In the chemical literature, empirical correlations can be found for small compounds that relate accurate C═O bond lengths to the stretching frequency, $\nu_{C=O}$.[7] In this way, it is estimated that the 54 $cm^{-1}$ downshift in $\nu_{C=O}$ seen in Figure 1 across the series corresponds to a bond lengthening of 0.025 Å.[8] This is equivalent to about 10% of the distance change going from a formal double bond C═O in the acyl enzyme to a single bond C—O in the transition state. Thus, in the ground state of the least stable acyl enzyme, we are "catching a glimpse" of the more radical changes that will occur in the transition state. The second insight that can gained from the data in Figure 1 relates to the strength of the active site forces, principally from the oxanion hole, that give rise to the shifts in $\nu_{C=O}$. The approach here is to use model compounds, e.g., 5MeTA methyl ester, and develop a relationship between hydrogen bonding strength at the C═O group and the downshift in its $\nu_{C=O}$. This is accomplished by using FTIR to study the equilibrium between monomers and hydrogen bonded complexes consisting of 5MeTA methyl ester and a hydrogen bonding donor in inert solvents such as $CCl_4$. Using the van't Hoff relationship, it was possible to estimate that the downshift in $\nu_{C=O}$ of 54 $cm^{-1}$ seen in Figure 1 corresponds to a change in the effective hydrogen bonding strength ($\Delta H$) of 57 kJ $mol^{-1}$.[9] Thus, the sum total of all active site forces acting on the acyl C═O is equivalent to a single H-bond with a $\Delta H$ of 57 kJ $mol^{-1}$. This represents the difference in these forces acting on the C═O in the least and most reactive acyl enzymes plotted in Figure 1.

Attempts at generating relationships for cysteine proteases similar to those seen in Figure 1 were unsuccessful.[10] This was due to the breakdown of the group frequency concept for the acyl's thioester carbonyl in the active site. As in the case of the serine proteases, non-natural acyl groups such as 5MeTA were used as active site probes. However, in the cysteine proteases, e.g. papain, the acyl groups experienced strong electric field effects that caused major rearrangement of the $\pi$-electrons. This led to a change in hybridization about the C═O carbon atom and vitiated the use of this group's stretching motion as a group frequency.

## 2.3. Meisenheimer Formation in a Dehalogenase

A second example features a relationship very similar to that seen in Figure 1, although the chemistry is completely different. The enzyme 4-chlorobenzoyl-CoA (4-CBA-CoA) dehalogenase catalyzes the hydrolytic dehalogenation of

4-CBA-CoA to 4-hydroxybenzoyl-CoA. In the reaction, the enzyme−substrate complex forms a Meisenheimer-like complex,[11] followed by $Cl^-$ expulsion and subsequent hydrolysis of the arylated enzyme (Scheme 1). The X-ray structure of the dehalogenase is known,[12] and this was used to design mutations that would impair interactions involving Gly 114 and Phe 64, making up the oxyanion hole (Scheme 1). This provided a series of mutants whose reactivities dropped by up to 2 400 000-fold.[13] Using single turnover kinetics, it was possible to derive the rate constants for the formation of the Meisenheimer complexes for each member of the series. Similarly, using substrate, in the case of the unreactive mutants, or substrate analogues, in the case of the more active forms of the enzyme, it was possible to undertake Raman difference spectroscopic analysis of (quasi)stable enzyme−substrate (pre-Meisenheimer) complexes, yielding the positions of the thiolester C═O stretching frequencies.[13] As can be seen in Figure 2, there is a good

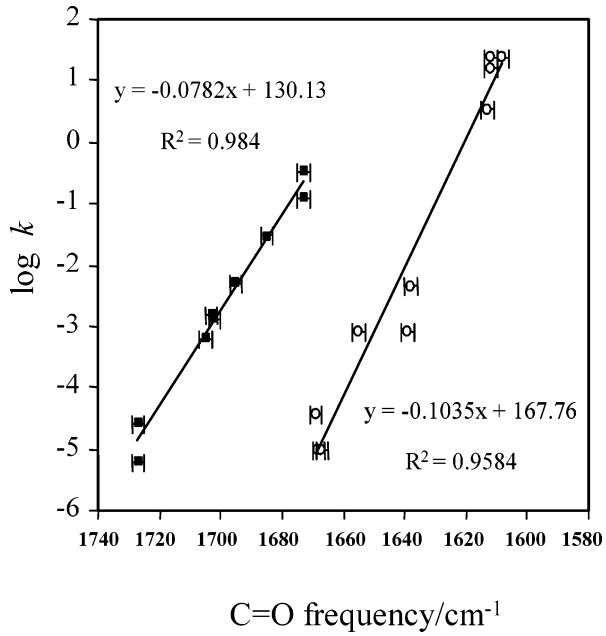


**Figure 2.** Correlation between carbonyl stretching frequencies and log *k* in two enzyme systems. Empty circles correspond to data for the 4-chlorobenzoyl-CoA dehalogenase series. Data for the serine protease series are shown as filled squares. Reprinted with permission from ref 13. Copyright 2003 American Chemical Society.

correlation between $\nu_{C=O}$ and $k_{obs}$, the rate of formation of the Meisenheimer complex, where the rate changes by 2 400 000-fold and $\nu_{C=O}$ changes by 61 $cm^{-1}$.

Figure 2 also includes the data for the serine proteases, and remarkably, there is close correspondence. For the dehalogenase, model studies, akin to those described above for the serine proteases, show that the change of $\nu_{C=O}$ by 61 $cm^{-1}$ corresponds to a change in effective hydrogen bonding strength of 67 kJ/mol. Taking the serine protease and dehalogenase results together, it can be shown that the log of rate acceleration per kilojoule per mole of hydrogen bonding strength is 0.074 for the acyl enzyme series and 0.095 for the dehalogenase series. This finding shows that a similar change in the effective H-bonding strength at the C═O group is associated with a similar degree of rate acceleration in both reactions. This is a remarkable conclusion considering the dissimilarities in chemistry—one reaction is nucleophilic substitution at an acyl C═O, while the other probes how interactions at the thiolester carbonyl modulate reactivity at a phenyl carbon atom five bonds away in a delocalized $\pi$-electron system.

## 2.4. Pyruvate in Lactate Dehydrogenase

One system used extensively by Callender, Deng, and coworkers to establish the power of Raman difference spectroscopy in enzymological studies is lactate dehydrogenase.[14] This enzyme accelerates the oxidation of lactate by $NAD^+$ to pyruvate and NADH by hydride transfer from the C-4 carbon of NAD to and from the cofactor. Aided by isotope editing in complexes of the enzyme with pyruvate and NAD, these workers probed, for example, the stereospecificity of hydride transfer and the energetics of substrate binding. In one set of studies, they were able to measure $\nu_{C=O}$ for pyruvate in the active site, where it undergoes strong interactions with the side chains His 195 and Arg 109. Using three mutant forms of the enzyme, wild-type (WT) data, and an estimate for the rate in solution, Deng et al. were able to demonstrate an approximate straight line relationship between the log of hydride transfer rate and the position of $\nu_{C=O}$ from the Raman difference data.[15] They took the standard state to be pyruvate in water, and compared to there, $\nu_{C=O}$ downshifts by about 35 $cm^{-1}$ in the WT enzyme. Their analysis determines that about 6 orders of magnitude of rate enhancement occurs as a result of the interactions that polarize the pyruvate C═O, with these interactions being optimized in the transition state.

## 2.5. Michaelis Complex in Liver Alcohol Dehydrogenase

Horse liver alcohol dehydrogenase (LADH) catalyzes the reactions of aldehydes and their corresponding alcohols with the coenzymes NADH and $NAD^+$. A complex between *N*-cyclohexylformamide, LADH, and NADH is taken as a mimic of the Michaelis complex for the true reaction.

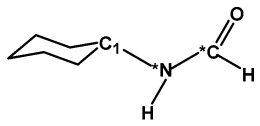


*N*-cyclohexylformamide

Using isotope editing ($^{13}C$ and $^{15}N$, shown by asterisks above) and Raman difference spectroscopy in solution, Deng and colleagues could identify the C═O stretching and N−H bending features of the bound formamide group.[16] The C═O stretching and N−H bending modes of the amide group shift −16 and −9 $cm^{-1}$, respectively, in the enzyme complex relative to those in aqueous solution and −48 and −36 $cm^{-1}$, respectively, relative to that in methylene chloride. Interpretation of these shifts was rendered complex due to the fact that interactions at the NH group affected $\nu_{C=O}$ and *vice versa.* However, based on *ab initio* calculations, Deng et al. were able to show that the portion of the shift in $\nu_{C=O}$ due to interactions at C═O could be distinguished and quantified. The authors developed an empirical relationship to relate this shift to a change in interaction enthalpy and found that the C═O group in the ternary complex binds with a favorable interaction enthalpy of 5.5 kcal/mol relative to water. The NH group, however, is destabilized in the ternary complex by 1.5 kcal/mol relative to water. Overall, the authors were able to provide a satisfying thermodynamic description of the interactions in the active site between the ligand's C═O group and the catalytic zinc and the hydroxyl group of Ser-48 and the interaction of the N−H with the benzene ring of

the active-site Phe-93. Such specific and quantitative information highlights the power of the Raman difference approach.

### 2.6. Uracil DNA Glycosylase—Distortion?

Uracil DNA glycosylase (UDG) recognizes a mismatched U−A base pair in a DNA sequence, flips out the uracil base, and excises it from the DNA strand. Raman difference studies provided information on each complex on the reaction pathway.[17] In particular, the Raman data for a specific complex between UDG and a DNA duplex containing 2′-$\beta$-fluorodeoxyuridine showed that the extrahelical uracil analogue underwent significant downshifts (34 $cm^{-1}$) in the carbonyl normal modes. However, the uracil ring modes were little perturbed by binding in UDG's active site. This result is at variance with the conclusion from a crystal structure, in which the UDG active site significantly distorts a flipped out pseudouridine analogue such that a change in hybridization at C1 occurs.[18] Such a change would constitute significant ground-state distortion and would almost certainly cause significant changes in the uracil ring modes. The Raman data were collected in solution, and Stivers and Drohat point out that one possible source of the discrepancy between the solution and crystal data is that in the crystal complex a tautomerization reaction may have occurred with the H3 proton being transferred to C1.[19] Further studies are needed to resolve this dichotomy, and clearly, these would use Raman crystallography to bridge solution and crystal data.[3]

## *3. Distortion at Phosphate and Vanadate Groups*

### 3.1. Bond Length–Bond Strength–Vibrational Frequency Relationships

Reactions involving the transfer or binding of phosphate groups occupy a central position in biochemistry. In many of these reactions, vanadate has found high utility in acting as a transition-state analogue for reactions using phosphate. Callender, Deng, and colleagues have demonstrated that exquisitely accurate geometric information can be obtained for both classes of compound using Raman difference spectroscopic and, more recently, FTIR measurements. Their approach relies on two empirical relationships that flow from the earlier findings of Badger and Bauer[20] and Gordy[21] that a characteristic stretching frequency may be related to bond strength. One relationship, developed by Brown and coworkers,[22] is a correlation relating bond length to bond strength:

$$s = (r/r_0)^p$$

where $s$ is the bond strength, $r$ is the bond length, and $r_0$ and $p$ are empirical parameters. The sum of bond strengths about the P or V atom for phosphate or vanadate in solution is equal to its oxidation state, which is 5 for both atoms.

Bond strength is also related to vibrational frequency by the Hardcastle and Wachs relationship[23] that takes the form

$$s = [a \ln(b/\nu)]^p$$

where, again, $a$, $b$, and $p$ are empirical parameters, and Deng et al.[24] found that the most useful form of the frequency $\nu$ is the so-called fundamental stretching frequency:

$$\nu = [(\nu_s^2 + d\nu_a^2)/(d+1)]^{1/2}$$

where $\nu_s$ and $\nu_a$ are the symmetric and antisymmetric stretches and $d$ is the degeneracy of the asymmetric modes. $\nu$ expressed in this manner depends directly on the P−O or V−O bond force constant and provides a more precise bond strength−frequency relationship.

### 3.2. Phosphoglucomutase

Phosphoglucomutase (PGM) catalyzes the reversible transfer of the $-PO_3^-$ group of a dianionic phosphate ester between the oxygens on the 1- and 6-positions of glucose. The reaction path is intricate and involves two binding and two transfer steps as well as rearrangement of an intermediate on the reaction pathway. Deng and co-workers uncovered marked differences in the binding properties of phosphate and a vanadate transition state analogue at the enzyme's proximal phosphate binding site.[25] These studies demonstrated the potential of Raman difference spectroscopy for characterizing phosphate binding sites within phosphoryl transfer proteins. Using isotope edited [$^{16}O/^{18}O$ at the phosphate] Raman difference spectra, it was possible to detect the symmetric stretching frequency of the PGM-bound phosphate group.[25] The observed frequency and its isotopic shift are characteristic of phosphate in its dianionic form. Moreover, the P−O stretching frequency is not perturbed by the binding of metal ion activators, $Mg^{2+}$, $Cd^{2+}$, or $Zn^{2+}$, or by subsequent binding of glucose phosphate. Hence, PGM's high degree of rate acceleration cannot be ascribed to ground-state distortion of the bound phosphate group. This situation is in marked contrast to that for the transition-state analogue vanadate binding at the proximal site.[25] In the difference spectrum seen in Figure 3, the vanadate stretching frequency for glucose 1-phosphate 6-vanadate bound to PGM is unusually low for a tetrahedral vanadate.

This is ascribed to the close approach of a fifth ligand, HOR′, which decreases the bond order of all three of the nonbridging V−O bonds:

$$RO-[VO_3^{2-}]\cdots O(H)R'$$

The polarization of the $VO_3^{2-}$ group is highly dependent on the bound metal since replacement of $Mg^{2+}$ by $Li^+$ largely removes polarization and thus the approach of the fifth ligand (Figure 3).

The relationships set out in section 3.1 can be used to calculate that the bond order of the three nonbridging V−O bonds changes from 1.37 vu (valence units) in solution to 1.20 vu in the $Mg^{2+}$−PGM complex. Since the sum of the bond orders about the V atom should be 5, there should be an increase in bond order of about 0.5 in the bridging and incipient V···O bonds. This enabled Deng et al. to suggest that the enzyme reaction involves an associative type mechanism, quite distinct from the dissociative process usually observed for model phosphate ester dianions in aqueous solution.[25]

Subsequently, the equations given in section 3.1 have been applied to other enzyme systems, as well as to analyze the environmental effects on phosphoryl group bonding in monosubstituted dianionic phosphates.[26] Raman difference spectroscopic studies of vanadate complexes have been used to probe the binding of transition-state analogues to myosin[27] and ribonuclease.[28] To provide information on antisymmetric phosphate modes, Callender's group have undertaken FTIR

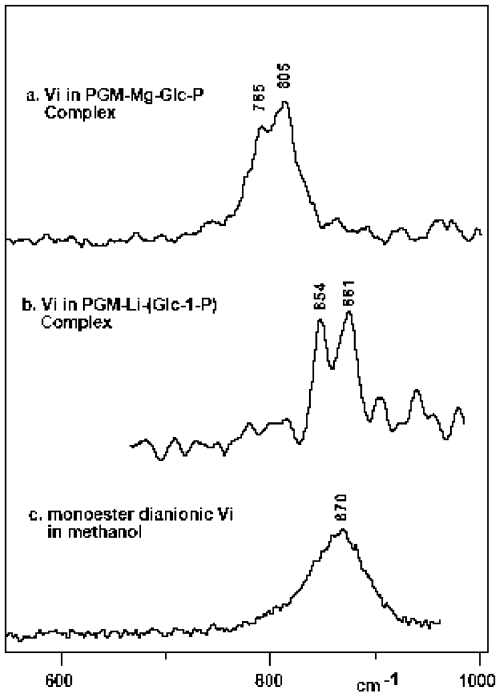


**Figure 3.** Raman spectra of (a) vanadate bound in the PGM·Glc-Vi complex, (b) vanadate bound in the PGM·Li·Glc-Vi complex, and (c) monoester dianionic methyl vanadate in methanol. Reprinted from *Methods in Enzymology*, Vol 308, H. Deng and R. Callender, Raman Spectroscopic Studies of the Structures, Energetics, and Bond Distortions of Substrates Bound to Enzymes, p 197, Copyright 1999, with permission from Elsevier.

studies of GDP and GTP binding to RAS;[29] this information supplements the Raman data that access the symmetric modes.[30] The two techniques provide exquisitely accurate information on changes in bond angles (on the order of 1−2°) and bond lengths (0.005 Å) upon active site binding.

## 3.3. Purine Nucleoside Phosphorylase

Purine nucleoside phosphorylase (PNP) catalyzes the phosphorolysis of inosine as depicted in Scheme 2. PNP is a target enzyme for the treatment of T-cell cancers and immunodeficiency diseases, and the inhibitor immuncillin-H (Scheme 2) was developed to resemble the transition state. The data from studies of PNP−immucillin H complexes could then be applied to the development of better inhibitors. Again, vibrational spectroscopy has been used to derive unprecedented structural detail from the part of the complex involving phosphate binding.[31] As can be seen in Figure 4,

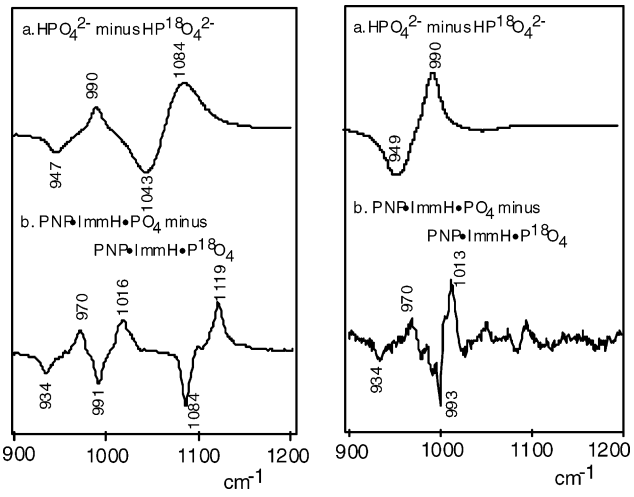


**Figure 4.** Difference FTIR (left panel) and difference Raman (right panel) spectra between $P^{16}O_4$ and $P^{18}O_4$ (a) in aqueous solution at pH 9.5 (dianionic) and (b) in the PNP·Imm·$PO_4$ complex. The positive bands are from $P^{16}O_4$, and the negative bands are from $P^{18}O_4$. Reprinted with permission from ref 31. Copyright 2004 American Chemical Society.

difference data were obtained using both FTIR and Raman spectroscopies. $HP^{16}O_4^{2-}$ or $HP^{18}O_4^{2-}$ was used in the original spectra from the complex PNP·ImmH·$PO_4^{2-}$, whereupon the subtraction [$HP^{16}O_4^{2-}$ complex] minus [$HP^{18}O_4^{2}$ complex] revealed the vibrational modes of the bound phosphate.

The modes seen in Figure 4 are in a spectral range consistent with the presence of $HPO_4^{2-}$, and $H_2PO_4^-$ can be eliminated as the bound species. However, the exact positions

**Scheme 2. PHP-Catalyzed Phosphorolysis of Inosine and the Interaction between Phosphate and the Transition-State Analogue Inhibitor ImmH in the PNP·ImmH·$PO_4$ Complex**

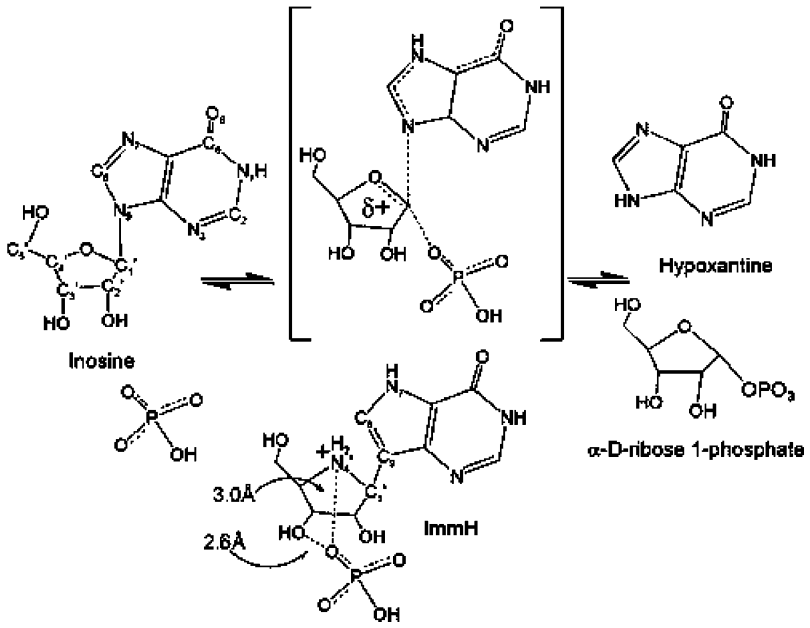

of the three P−O stretching modes seen for the unlabeled complex at 970, 1016, and 1119 $cm^{-1}$ in the FTIR spectra in Figure 4 are unusual and indicate a highly distorted phosphate group. The distortion takes the form of one of the three P−O bonds being strongly polarized by active site forces; this causes its stretch motion to be decoupled from the P−O stretches of its two neighbors. The uncoupled P−O stretch is active in both the Raman and IR spectra, while the other two P−O stretches are coupled to form an IR-active asymmetric stretch and an IR-active and Raman-active symmetric stretch. The authors favor assigning the mode at 970 $cm^{-1}$ to the uncoupled P−O stretch and the 1016 and 1119 $cm^{-1}$ features to the symmetric and antisymmetric motions of the coupled P−O bonds. Based on the relationships enunciated in section 3.1, this gives a bond length of 1.543 Å for the polarized P−O bond compared to 1.516 Å for the coupled nonpolarized bonds. The increase in 0.027 Å for the polarized bond represents an excursion of about 20−25% toward the bridging P−O−C bond (Scheme 2).

## *4. Distortion within π-Electron Systems*

### 4.1. Acyl Papains

Many ligands, for example, cofactors or substrates, have extended delocalized $\pi$-electron systems. As a consequence, these ligands are colored due to low lying $\pi \rightarrow \pi^*$ transitions in the visible region of the electronic spectrum. Early attempts were made to relate shifts in the absorption maxima, especially "red shifts", to enzyme rate acceleration.[32] However, quantitation was hampered by the fact that absorption bands are a property of electronic ground and excited states, whereas most reactions occur in the ground state only. Moreover, an absorption maximum is a property of an extended molecular region and offers little information at the level of individual bonds. This situation underwent a sea change with the application of resonance Raman (RR) spectroscopy to enzyme−substrate systems that featured naturally chromophoric substrates or substrates that had been labeled to become chromophoric.[33] We have already seen (section 2.2) that the RR approach enabled the characterization of an individual C═O bond in the active site during the catalytic step that involved hydrolysis of an acyl enzyme intermediate. In this class of enzyme intermediates, based on serine proteases, the substrate group underwent a modest change in absorption maximum and RR spectrum upon binding to the enzyme. However, for similar experiments employing the cysteine protease papain, much larger red shifts were observed for the acyl enzyme and these were accompanied by a total reorganization of the substrate's RR spectrum.[34] These spectroscopic effects were ascribed to major changes in the distribution of $\pi$-electrons in the bound acyl group due to strong electric charge (or dipole) effects in the active site. In effect, the acyl group becomes more quinonoid-like, with contributions from valence bond structure II becoming more important.[35]

### 4.2. Acyl Thiosubtilisn and Selenosubtilisin

In the above studies, $\pi$-electron polarization was assisted by the choice of acyl group—where the strong electron donating ability of the 4-dimethylamino group provides "internal assistance" to polarization. Subsequent studies in two areas, with the semisynthetic enzymes thio- and selenosubtilisin and with 4-chlorobenzoate CoA dehalogenase,

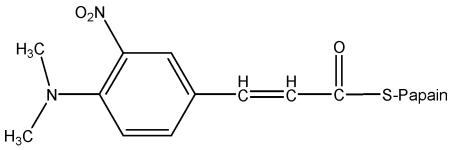


**I**

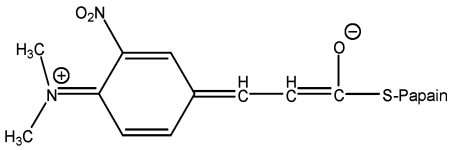


**II**

have shown that electron push near the end of the acyl tail can equally well be provided by a negatively charged protein side chain. The work with the subtilisin derivatives used the substrate 5-methylthienyl-acryloyl (5-MTA) imidazole, forming acyl ezymes of the kind

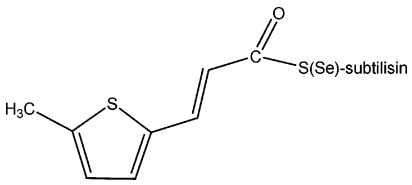


The intermediates have absorption maxima in the 350−370 nm region and gave high quality preresonance Raman spectra using 488 nm excitation.[36] In this class of acyl enzymes (including papain), the C═O region is not informative since extensive rehybridization of the group occurs in the active site. However, the stretching frequency $\nu_{C=C}$ is an intense and useful marker band. As can be seen in Table 1 red shifts

**Table 1. $\lambda_{max}$ and $\nu_{C=C}$ for 5-Methylthienylacryloyl (5-MTA) in Various Forms**

| compound | $\lambda_{max}$ (nm) | $\nu_{C=C}$ ($cm^{-1}$) |
|---|---|---|
| 5-MTA acid (in $CCl_4$) | 324 | 1623 |
| acyl chymotrypsin | 332 | 1615 |
| 5-MTA thiolester (in $CCl_4$) | 338 | 1601 |
| acyl papain | 385 | 1576 |
| acyl thiolsubtilisin (pH 9.6) | 350 | 1606 |
| acyl P225A thiolsubtilisin | 361 | 1601, 1577 |
| acyl selenosubtilisin (pH 9.6) | 355 | 1584 |

in the 5-MTA chromophore are accompanied by downshifts in $\nu_{C=C}$'s.

In both 5-MTA-S-subtilisin and 5-MTA-Se-subtilisin, there is only minor $\pi$-electron polarization in the 5-MTA group which is present as the *s-trans* form about the ═C−C═O single bond. However, when the active sites are enlarged by mutagenesis, a second conformational form appears. Figure 5 compares the Raman difference spectra for 5-MTA bound to "WT" thiolsubtilisin and the form that has its active site enlarged by the substitution P225A (bottom of Figure 5).

In the latter, a second $\nu_{C=C}$ feature appears at 1577 $cm^{-1}$. Based on quantum mechanical and molecular modeling calculations, the new feature was assigned to a second conformational population *s-cis* about the ═C−C═O single bond. Interestingly, the *s-cis* form now has its $\pi$-electrons highly polarized by active site forces. This is an example of how a simple conformational change in an active site can

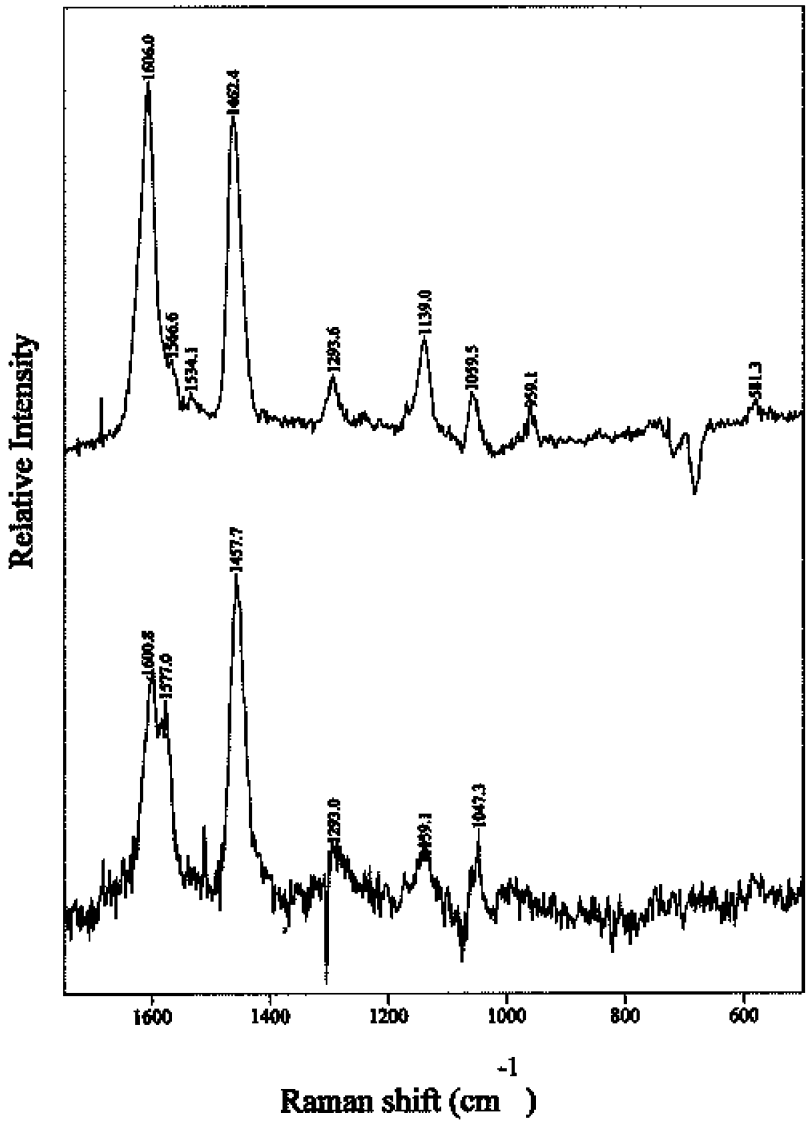


**Figure 5.** Raman difference spectra of 5-methylthienylacryloyl thiolsubtilisin: (a, top) acyl derivative of native thiolsubtilisin; (b, bottom) acyl derivative of P225A thiolsubtilisin. Note the additional feature near 1577 $cm^{-1}$ in the lower spectrum. Reprinted with permission from ref 36. Copyright 1999 American Chemical Society.

take a ligand from a site with no electric fields to one where strong polarizing forces come into play.

The results for papain, thiol- and selenosubtilisin, and dehalogenase all lead to a simple model for "strong electron polarization" in the active site:

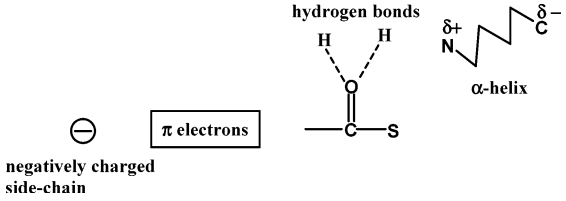


For the papain family, electron pull at the C═O group is brought about by hydrogen bonding to the two −NH groups in the oxyanion hole and by the dipole due to an adjacent α-helix. These forces stabilize charge buildup in the tetrahedral intermediate. Similar forces acting on the C═O group in 4-chlorobenzoate-CoA dehaogenase are transmitted through the $\pi$-electron chain to reduce electron density at the *para*-position and to assist in the formation of the Meisenheimer intermediate.[13]

## 4.3. Contribution of Electronic Strain in Enoyl-CoA Hydratase

Enoyl-CoA hydratase hydrates the C═C bond in $\alpha,\beta$-unsaturated esters bound to CoA:

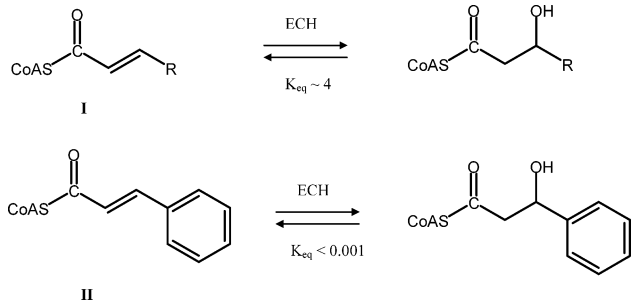


Anderson and co-workers[37] found that, by extending conjugation by adding a phenyl ring (compound II), stable enzyme−"substrate" complexes could be formed that were amenable to spectroscopic characterization. A large red shift in the absorption maximum, alternating changes in $^{13}C$ chemical shielding, and downshifts of the Raman C═O

stretch and the C═C stretch all indicated substantial polarization in the $\pi$-electron chain for the bound substrate analogue in the direction that would enhance its reactivity. Anderson then calculated the degree of electron strain (or polarization) in this system. Although the shifts in spectroscopic properties were large, he found the changes in electron densities were small, typically $<0.01$ e/Å$^3$. Moreover, Anderson reasoned that a calculation of the difference in electronic energy for the substrate analogue in the presence and absence of the electric field in the active site, without allowing the conformation to relax, would provide an estimate of ground-state electronic strain.[37] This was found to be 3.2 kcal/mol. If all this strain is released in the transition state, it can make a significant, but only partial, contribution to the catalytic power of the enzyme.

## 5. Distortion Involving Torsional Angles

For GDP and GTP binding to RAS, we have seen in section 3.2 that Cheng et al.[29] could define small changes (on the order of a few degrees) in phosphate valence angles by using IR and Raman data as the reference points for the calculations. Since torsional (dihedral) angles often require only a modest application of force to distort them from equilibrium values, comparatively larger changes are often found in ligand torsional angles upon binding to enzymes. The next section discusses the use of resonance Raman studies on dithioacyl papains to map the Ramachandran-like angles for the bound substrate and to demonstrate that torsional angle distortion occurs in the direction predicted for the reaction pathway. The final section deals with complex reaction intermediates between antibiotic-like compounds and a $\beta$-lactamase. These studies show that clinically effective inhibitors can still have energetically unfavorable distortion in the active site.

### 5.1. Distortion toward the Transition State in Dithioacyl Papains

By reacting substrates which are thionoesters, e.g., $RC(=O)NHCH_2C(=S)OCH_3$, with cysteine proteases such as papain, it is possible to generate dithioacyl enzymes, $RC(=O)NHCH_2C(=S)SCH_2$-papain, in which the thiol sulfur is donated by papain's cysteine 25. The dithioester group in the active site has a $\lambda_{max}$ near 315 nm, and excitation of the reaction mixture with 324-nm krypton laser irradiation generates the resonance Raman (RR) spectrum of the dithioester moiety.[38] By these means, it is possible to observe selectively the vibrational spectrum of the group undergoing transformation in the active site. The RR data are gathered from the reaction mixture under turnover conditions, and principally, the spectra provide information on the torsional angles $\varphi'$, $\psi'$, $\chi_2$, and $\chi_1$ seen in Figure 6.

X-ray and RR studies of model compounds, consisting of six *N*-acylglycine ethyl dithioesters, were used to set up structure−RR spectra correlations. Moreover, the X-ray analysis revealed a strong correlation between structural parameters in the $-NHCH_2C(=S)SCH_2CH_3$ core. Figure 7 plots the relationship between the Ramachandran-like angle $\psi'$ and two prominent features in the dithioester RR spectra of the six model compounds. In the RR spectrum of the reaction intermediate *N*-benzoylglycine dithioacyl papain, these features occur at 1127 and 558 cm$^{-1}$, and plotting the values on the model-derived correlation provides a value of $+15°$ for $\psi'$ in the functioning dithioacyl enzyme. This value

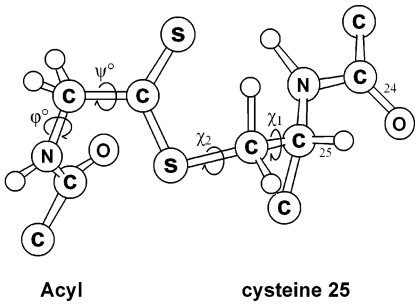


**Figure 6.** View defining the torsional angles of the glycine−cysteine bonds in the active site of a dithioacyl papain intermediate. Reprinted with permission from ref 38. Copyright 1993 American Chemical Society.

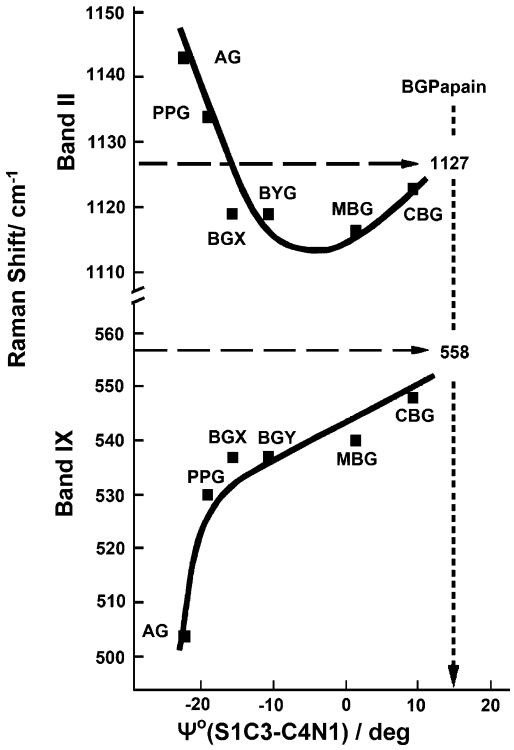


**Figure 7.** Variations of two Raman marker bands relative to the torsion angle $\psi'$ (Figure 6) for six different single crystals of *N*-acylglycine ethyl dithioesters: AG, *N*-acetylglycine ethyl dithioester; PPG, *N*-($\beta$-phenylpropionyl) gylcine ethyl dithioester; BGX and BGY are two forms of *N*-benzoylglycine ethyldithioester; MBG, *N*-(*p*-methylbenzoyl)glycine ethyl dithioester; CBG, *N*-(*p*-chlorobenzoyl)glycine ethyl dithioester. The positions of the marker bands for *N*-benzoylgylcine dithiopapain (BGPapain) indicate that $\psi'$ for this species is distorted toward that for the transition state. Reprinted with permission from ref 38. Copyright 1993 American Chemical Society.

is outside the range, $-22$ to $+9°$, seen for the model compounds in the crystalline state. In the tetrahedral intermediate for deacylation, $\psi'$ assumes a value of $+60°$;[38] therefore, it is apparent that, in the dithioacyl enzyme, enzyme−substrate contacts are bringing about a small but significant departure of $\psi'$ in the direction of that found near the transition state. A further consequence of an increase in $\psi'$ is that it weakens the favorable interaction between the glycine N atom and the thiol sulfur, thereby reducing the stability of the dithioacyl enzyme.

Another way in which enzyme active sites manipulate torsional angles involves selecting a favorable substrate conformation from a number of states that are nearly redundant in energetic terms. Chen et al.[39] found that this is

**Scheme 3. Structures of β-Lactamase Inhibitors**

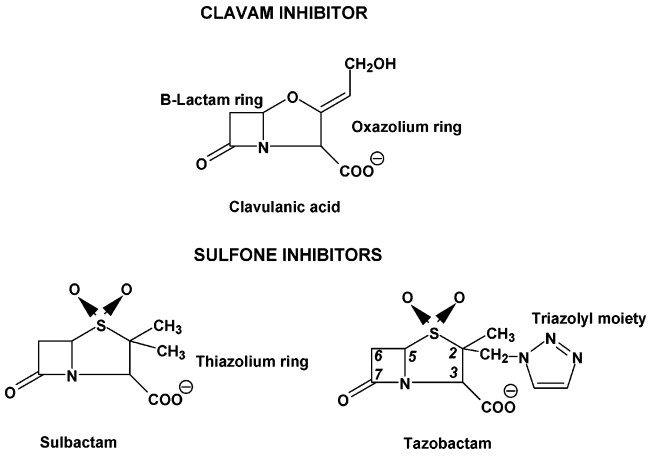


a common factor for NAD(P)H and $NADP^+$ binding to three NAD(P) dependent enzymes. These authors used the vibrational structure of the cofactors labeled with C4-D at the *pro-R* or *pro-S* of the reduced ring or the C4 hydrogen of the oxidized ring. The deuterium substitution allowed access to the properties of the individual C−D bond in complexes with lactate dehydrogenase (LDH), dihydrofolate reductase, and glycerol-3-phosphate dehydrogenase. An important general finding was that that binding brought about significant narrowing of the C−D stretching profile. Thus, for NADH, the bandwidth at half-height for the labeled C−D stretch is 45 $cm^{-1}$ in solution, 16 $cm^{-1}$ in the binary complex with LDH, and just 6 $cm^{-1}$ in the ternary complex. This band narrowing was ascribed to a decrease in the freedom of thermomotion about a specific cofactor conformation. In other words, the enzyme-binding site is forcing the cofactor to adopt a narrower range of torsional angles.

## 5.2. Distortion in a β-Lactamase–Tazobactam Reaction Intermediate

This project uses Raman microscopy combined with X-ray crystallography to investigate the mechanism of drug resistance in penicillin-based antibacterial therapy. Penicillin-like compounds kill bacteria by interfering with cell wall synthesis, but bacteria produce enzymes, β-lactamases, which hydrolyze the penicillin before it can damage the cells. Thus, in modern therapy, a second drug is coadministered with the penicillin-like compound in order to inhibit the action of the β-lactamases. Unfortunately, the bacteria then produce mutant forms of the β-lactamase, often differing by a single amino acid change, that are no longer inhibited by the lactamase directed inhibitor. The three clinically used inhibitors of class A β-lactamases are tazobactam, sulbactam, and clavulanic acid (Scheme 3). These undergo a complex reaction with the enzyme that includes a number of reaction intermediates.[40] The objective is to compare the reactions and reaction intermediates for wild-type β-lactamase and drug-resistant forms, thereby to determine the molecular basis of drug resistance. The reactions are fairly slow, on the time scale of seconds to minutes, and it was found recently that the reactions could be followed in single crystals of the enzyme by Raman microscopy.[41] This has two advantages, the crystals provide Raman spectra of the intermediates that are of unprecedented quality, and these data provide an immediate link to X-ray crystallography.[42] Intermediate populations identified by "Raman crystallography" can be flash frozen and characterized by X-ray crystallography.

The Raman difference spectra shown in Figure 8 were recorded using a Raman microscope with red (647 nm) excitation. The top trace is for free tazobactam in solution, while the middle and bottom traces were recorded from crystals at 2 and 28 min, respectively, after tazobactam was infused into single crystals of SHV-1 β-lactamase. The enzyme carried the site specific mutation E166A that essentially trapped the acyl enzyme formed on the reaction pathway.

For the crystal Raman data the difference spectra contain few modes that can be assigned to the parent tazobactam. Key observations are that peaks near 1780 $cm^{-1}$, due to the β-lactam C═O, and at 625 $cm^{-1}$, due to a C−S mode from the thiazolium ring, are absent, showing that both rings have opened upon reaction in the enzyme's active site. A peak near 1593 $cm^{-1}$ grows with time, and analysis assigned this to the totally symmetric double bond stretching frequency

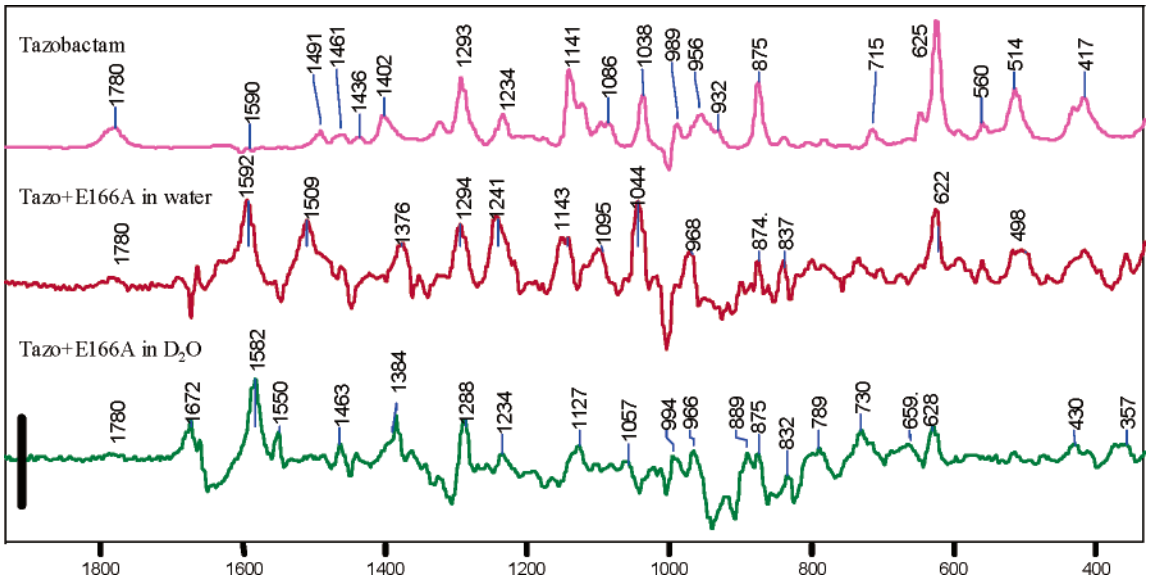


**Figure 8.** Raman difference spectra of free tazobactam (top trace) and tazobactam soaking into an E166A β-lactamase crystal at different times (middle and bottom traces). The vertical bar denotes a 2000-photon event. Reprinted with permission from ref 41. Copyright 2003 American Chemical Society.

of a *trans*-enamine species postulated to form on the reaction pathway:

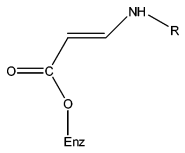


*Trans* enamine

All three inhibitors exhibited a peak in this region, and by plotting standardized peak intensities, it is possible to follow population changes in the intermediates within the crystal (Figure 9). Interestingly, tazobactam, the compound with the

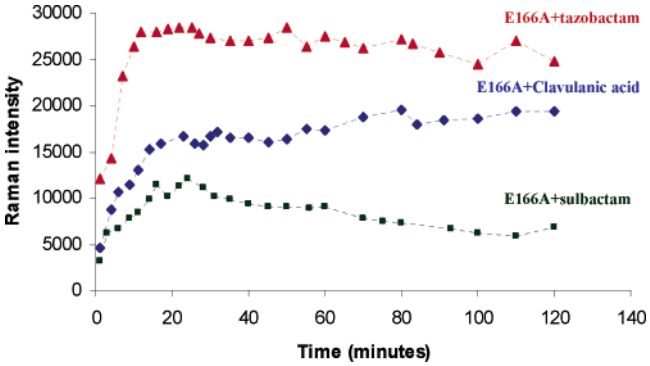


**Figure 9.** Time dependence of enamine peak area near 1593 $cm^{-1}$ (normalized to amide I band) for the E166A crystal and three inhibitors: (red triangles) tazobactam; (green squares) sulbactam; (blue diamonds) clavulanic acid. Reprinted with permission from ref 41. Copyright 2003 American Chemical Society.

greatest clinical efficacy, has the highest population of *trans*-enamine in the crystal, leading to the hypothesis that this species may play a key role in blocking the enzyme's active site.

The Raman population data seen in Figure 9 are of great value in setting conditions for flash freezing the crystal at the time of optimal intermediate buildup, to obtain structural data by X-ray crystallographic analysis. Structures have been obtained for intermediates formed from all three inhibitors.[42,43] A cartoon of the active site for the *trans*-enamine formed from tazobactam[42] is seen in Figure 10. The structure

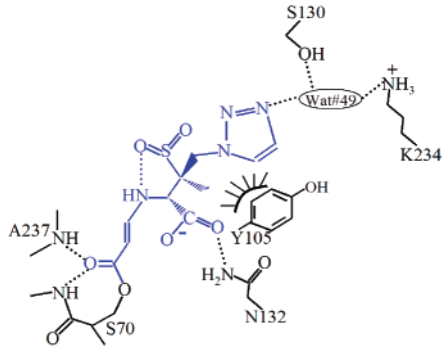


**Figure 10.** Diagram of tazobactam bound to the E166A mutant of SHV-1 $\beta$-lactamase. Hydrogen bonds are indicated as dotted lines, and the hydrophobic van der Waals interactions between Y105 and the triazole ring and methyl moieties of tazobactam are depicted with the hatched curved line. Reprinted with permission from ref 42. Copyright 2004 American Chemical Society.

has well resolved electron density and shows favorable contacts involving active site side chains. Some of these contacts need, for example, the triazole ring and, thus, cannot be duplicated for sulbactam or clavulanic acid.[43] Consequently, there is disorder in the enamine "tails" for the later two compounds, resulting both in a smearing of electron density and in a broadening of Raman line shapes.[43]

The favorable contacts seen in Figure 10 increase the stability of the intermediate and explain the higher active site occupancy of the tazobactam derivative. Interestingly, though, this comes with a cost. Table 2 compares the C—C═C—N torsional angles for the three *trans*-enamine species as well as the position of the double bond stretching frequency.

**Table 2. C—C═C—N Torsional Angles and the Totally Symmetric Stretching Frequency "$\nu_{C=C}$" for the *trans*-Enamine Complexes of E166A $\beta$-Lactamase with the Three Inhibitors**

| | C—C═C—N torsional angle (deg) | $\nu_{C=C}$ ($cm^{-1}$) |
|---|---|---|
| tazobactam | 168 | 1593 |
| sulbactam | −172 | 1599 |
| clavulanic acid | 180 | 1606 |

The geometry about the double bond is planar for the clavulanic acid-based intermediate, but the tazobactam-based species shows significant distortion, being 12° twisted from planarity. This provides an explanation as to why its stretching frequency at 1593 $cm^{-1}$ is lower than that for the clavulanic acid derivative at 1606 $cm^{-1}$. Slight twisting about the double bond reduces $\pi$-orbital overlap and the force constant associated with the mode, and this will reduce the frequency. Thus, the best inhibitor does have some energetically unfavorable distortion, but this is obviously outweighed by the favorable acyl group—active site contacts that are seen in Figure 10.

## 6. Acknowledgments

It is a great pleasure to acknowledge the vital contributions made to the author's research by many colleagues and coworkers. Their names appear in the list of references. At present the author's laboratory is supported by the NIH (Grants GM 54072 and DK 53053).

## 7. References

(1) Karplus, P. A. *Protein Sci.* **1996**, *5*, 1406.
(2) Herzfeld, J.; Lansing, J. C. *Annu. Rev. Biophys. Biomol. Struct.* **2002**, *31*, 73.
(3) Carey, P. R.; Dong, J. *Biochemistry* **2004**, *43*, 8885.
(4) Belasco, J. G.; Knowles, J. R. *Biochemistry* **1980**, *19*, 472.
(5) MacClement, B. A. E.; Carriere, R. G.; Phelps, D. J.; Carey, P. R. *Biochemistry* **1981**, *20*, 3438.
(6) Carey, P. R.; Tonge, P. J. *Acc. Chem. Res.* **1995**, *28*, 8.
(7) Horvath, G.; Illenyi, J.; Pusztay, L.; Simon, K. *Acta Chim. Hung.* **1987**, *124*, 819.
(8) Tonge, P. J.; Carey, P. R. *Biochemistry* **1992**, *31*, 9122.
(9) Tonge, P. J.; Fausto, R.; Carey, P. R. *J. Mol. Struct.* **1996**, *379*, 135.
(10) Doran, J. D.; Carey, P. R. *Biochemistry* **1996**, *35*, 12495.
(11) Dong, J.; Carey, P. R.; Wei, Y.; Luo, L.; Lu, X.; Liu, R.-Q.; Dunaway-Mariano, D. *Biochemistry* **2002**, *41*, 7453.
(12) Benning, M. M.; Taylor, K. T.; Liu, R.-Q.; Yang, G.; Xiang, H.; Wesenberg, G.; Dunaway-Mariano, D.; Holden, H. M. *Biochemistry* **1996**, *35*, 8103.
(13) Dong, J.; Lu, X.; Wei, Y.; Luo, L.; Dunaway-Mariano, D.; Carey, P. R. *Biochemistry* **2003**, *42*, 9482.
(14) Deng, H.; Callender, R. *Methods Enzymol.* **1999**, *308*, 176.
(15) Deng, H.; Zheng, J.; Clarke, A.; Holbrook, J. J.; Callender, R.; Burgner, J. W. *Biochemistry* **1994**, *33*, 2297.
(16) Deng, H.; Schindler, J. F.; Berst, K. B.; Plapp, B. V.; Callender, R. *Biochemistry* **1998**, *37*, 14267.
(17) Dong, J.; Drohat, A. C.; Stivers, J. T.; Pankiewicz, K. W.; Carey, P. R. *Biochemistry* **2000**, *43*, 13241.

(18) Parikh, S. S.; Walcher, G.; Jones, G. D.; Slupphaug, G.; Krokan, H. E.; Blackburn, G. M.; Tainer, J. A. *Proc. Natl. Acad. Sci., U.S.A.* **2000**, *97*, 5083.
(19) Stivers, J. T.; Drohat, A. C. *Arch. Biochem. Biophys.* **2001**, *396*, 1.
(20) Badger, R. M.; Bauer, S. H. *J. Chem. Phys.* **1937**, *5*, 839.
(21) Gordy, W. J. *J. Chem. Phys.* **1946**, *14*, 305.
(22) Brown, I. D.; Wu, K. K. *Acta Crystallogr.* **1976**, *B32*, 1957.
(23) Hardcastle, F. D.; Wachs, I. E. *J. Raman Spectrosc.* **1990**, *21*, 683.
(24) Deng, H.; Wang, J.; Callender, R.; Ray, W. J. *J. Phys. Chem. B* **1998**, *102*, 3617.
(25) Deng, H.; Ray, W. J.; Burgner, J. W.; Callender, R. *Biochemistry* **1993**, *32*, 12984.
(26) Cheng, H.; Nikolic-Hughes, I.; Wang, J. H.; Deng, H.; O'Brien, P. J.; Wu, L.; Zhang, Z.-Y.; Herschlag, D.; Callender, R. *J. Am. Chem. Soc.* **2002**, *124*, 11295.
(27) Deng, H.; Wang, J.; Callender, R. H.; Grammer, J. C.; Yount, R. G. *Biochemistry* **1998**, *37*, 10972.
(28) Deng, H.; Burgner, J. W.; Callender, R. H. *J. Am. Chem. Soc.* **1998**, *120*, 4717.
(29) Cheng, H.; Sukal, S.; Deng, H.; Leyh, T. S.; Callender, R. *Biochemistry* **2001**, *40*, 4035.
(30) Wang, J. H.; Xiao, D. G.; Deng, H.; Webb, M. R.; Callender, R. *Biochemistry* **1998**, *37*, 11106.
(31) Deng, H.; Lewandowicz, A.; Schramm, V. L.; Callender, R. *J. Am. Chem. Soc.* **2004**, *126*, 9516.
(32) Bernard, S. A.; Lau, S.-J. *Cold Spring Harbor Symp. Quant. Biol.* **1972**, *36*, 75.
(33) Carey, P. R.; Schneider, H. *Acc. Chem. Res.* **1978**, *11*, 122.
(34) Carey, P. R.; Carriere, R. G.; Phelps, D. J.; Schneider, H. *Biochemistry* **1978**, *17*, 1081.
(35) Carey, P. R.; Tonge, P. J. *Chem. Soc. Rev.* **1990**, *19*, 293.
(36) Dinakarpandian, D.; Shenoy, B. C.; Hilvert, D.; McRee, D. E.; McTigue, M.; Carey, P. R. *Biochemistry* **1999**, *38*, 6659.
(37) Anderson, V. E. *Arch. Biochem. Biophys.* **2005**, *433*, 27.
(38) Kim, M.; Birnbaum, G. I.; Hynes, R. C.; Neugebauer, W.; Carey, P. R. *J. Am. Chem. Soc.* **1993**, *115*, 6230.
(39) Chen, Y.-Q.; van Beck, J.; Deng, H.; Burgner, J.; Callender, R. *J. Phys. Chem. B* **2002**, *106*, 10733.
(40) Page, M. G. P. *Drug Resist. Updates* **2000**, *3*, 109.
(41) Helfand, M. S.; Totir, M. A.; Carey, M. P.; Hujer, A. M.; Bonomo, R. A.; Carey, P. R. *Biochemistry* **2003**, *42*, 13386.
(42) Padayatti, P. S.; Helfand, M. S.; Totir, M. A.; Carey, M. P.; Hujer, A. M.; Carey, P. R.; Bonomo, R. A.; van den Akker, F. *Biochemistry* **2004**, *43*, 843.
(43) Padayatti, P. S.; Helfand, M. S.; Totir, M. A.; Carey, M. P.; Carey, P. R.; Bonomo, R. A.; van den Akker, F. *J. Biol. Chem.* **2005**, *280*, 34900.

CR0502854